10 March 2026

A Zn4L4 cage with guest-programmable stereochemistry

Itai Massad[1], Anshuman Agarwal[1], Charlotte Lefebvre[2], Paula C P Teeuwen[1], Tanya K Ronson[1], Pascal Gerbaux[2], Quentin Duez[2], Jonathan R Nitschke[1]

1. Yusuf Hamied Department of Chemistry University of Cambridge

2. Organic Synthesis and Mass Spectrometry Laboratory University of Mons

Abstract

Supramolecular hosts with flexible and controllable shapes offer the prospect of generating new technologies, for example in selective chemical purifications. However, balancing flexibility with the rigidity and fidelity required for successful assembly and guest recognition needed for purification applications remains challenging. Here we report a Zn4L4 tetrahedral cage that interconverts between four diastereomers, driven by binding different guest molecules. The truxene-based cage backbone features inward-pointing methyl groups that enclose guests and differentiate the cavities of otherwise similar diastereomers. The cage switches quantitatively between two T-symmetric diastereomers when exposed to adamantane in varying stoichiometry, and adopts C3-or C2-symmetric diastereomers in the presence of lower-symmetry guests. Cyclic ion-mobility mass spectrometry (cIMS-MS) provided insights into the structure and dynamics of these diastereomeric host-guest complexes, indicating that the cage can retain its stereochemistry following guest release. We leveraged this "shape-memory" effect to achieve the programmable binding of different guests from a mixture, as controlled by pre-programmed host stereochemistry.

https://doi.org/10.26434/chemrxiv.15000792/v1

A Zn_4L_4 cage with guest-programmable stereochemistry

Itai Massad,[1] Anshuman Agarwal,[1] Charlotte Lefebvre,[2] Paula C. P. Teeuwen,[1] Tanya K. Ronson[1], Pascal Gerbaux[2], Quentin Duez[2]* and Jonathan R. Nitschke[1]*

[1]Yusuf Hamied Department of Chemistry, University of Cambridge, Cambridge, UK.

[2]Organic Synthesis and Mass Spectrometry Laboratory, University of Mons, Belgium.

Abstract

Supramolecular hosts with flexible and controllable shapes offer the prospect of generating new technologies, for example in selective chemical purifications. However, balancing flexibility with the rigidity and fidelity required for successful assembly and guest recognition needed for purification applications remains challenging. Here we report a Zn_4L_4 tetrahedral cage that interconverts between four diastereomers, driven by binding different guest molecules. The truxene-based cage backbone features inward-pointing methyl groups that enclose guests and differentiate the cavities of otherwise similar diastereomers. The cage switches quantitatively between two *T*-symmetric diastereomers when exposed to adamantane in varying stoichiometry, and adopts C_3- or C_2-symmetric diastereomers in the presence of lower-symmetry guests. Cyclic ion-mobility mass spectrometry (cIMS-MS) provided insights into the structure and dynamics of these diastereomeric host-guest complexes, indicating that the cage can retain its stereochemistry following guest release. We leveraged this "shape-memory" effect to achieve the programmable binding of different guests from a mixture, as controlled by pre-programmed host stereochemistry.

Introduction

Metal-organic cages often display intricate stereochemistry, which emerges from the confluence of multiple interconnected stereogenic units such as octahedral[1] and tetrahedral[2] metal ions, chiral ligands,[3-9] and low-symmetry ligands capable of assuming multiple different orientations in the cage framework.[10-20] Although cages are usually designed to adopt a single, highly symmetrical stereoisomer,[21-23] cages with intrinsic stereochemical flexibility[24] present attractive features as supramolecular hosts, as they can modulate their cavity to optimize guest binding,[25-27] enabling high-affinity binding to a broad scope of guests.[28]

Several design strategies have been developed to construct robust, yet stereochemically flexible, metal-organic cages. These include structures where the metal vertices can change their relative stereochemistry,[29-32] heteroleptic assemblies where rectangular ligand panels can change their orientation,[14] or cages based on conformationally flexible ligands.[28]

Although the adaptive guest-binding of flexible hosts is fundamentally interesting, their application in chemical purification[33] would require that they selectively and predictably extract a specific cargo from a mixture, rather than constantly rearrange to bind multiple different guests in competition. The dynamic nature of flexible hosts must therefore be balanced with structural fidelity that prevents information loss, such that the host adopts a specific shape and retains it, leading to selective guest recognition.

Here, we investigate the stereochemical plasticity of homoleptic Zn_4L_4 tetrahedron **1**—structurally much simpler than previously reported flexible hosts—that selectively interconverts between four different diastereomers, as templated by guest molecules. The small degree of offset in the truxene-centered ligand backbone allows both *clockwise* and *anticlockwise*-oriented faces to be incorporated into the structure without incurring prohibitive levels of strain, while endohedral methyl groups[34, 35] differentiate the cavities of the resulting diastereomers. Each isomer thus displays shape complementarity to different guests, resulting in highly selective templation. We show that the

stereochemistry dictated by a guest can be retained following its release, enabling the controlled binding of different guests from a mixture by pre-programming the stereochemistry of the host.

Results and discussion

Host **1**, a Zn_4L_4 tetrahedron, was assembled from hexamethylated truxene trianiline subcomponent $\mathbf{A^{Me}}$, 2-formylpyridine and $Zn(NTf_2)_2$ in acetonitrile (Figure 1a). We have recently investigated the contrasting stereochemical preferences of **1** and **2**, its ethyl congener: **2** adopts a *T*-symmetric structure with Δ_4AC_4 (*AC*– anticlockwise, Figure 1b) relative stereochemistry, labelled $\boldsymbol{T_S}$,[36] which features minimal backbone strain and cavity size, whereas **1** favors the Δ_4C_4 diastereomer, labelled $\boldsymbol{T_L}$, which is stabilized by attractive head-to-head Me-Me contacts.[37] The ^{1}H NMR spectra of the two cages (Figure 1c) reflect this stereochemical dichotomy, featuring distinct chemical shifts consistent with different *T*-symmetric frameworks. Furthermore, along with the signals corresponding to the major *T*-symmetric isomer, the ^{1}H NMR spectrum of **1** reveals several minor, low-symmetry diastereomers, as indicated by splitting of the ligand protons into multiple non-equivalent environments. The imine region of the spectrum contains 14 discernible singlets, which correspond to at least four coexisting diastereomers (Supporting Information, section 2). Hypothetically, the structures of these minor low-symmetry isomers may contain a combination of *Δ*- and *Λ*-configured metal vertices, and/or a combination of *C*- and *AC*-configured truxene faces. Evidence presented below supports the latter possibility—the low-symmetry isomers feature homochiral metals and heterochiral faces, as listed in Figure 1b.

Each diastereomer of **1** encloses a cavity of distinct size and shape, defined by the geometry of the cage backbone and further accentuated by the endohedral methyl groups (Figure S118). The subtle stereochemical balance **1** exhibits might therefore respond to the presence of guest molecules, which could drive it to preferentially express the optimally binding diastereomer. Indeed, when 1 equivalent of adamantane (**G1**) was added to a solution of **1** in CD_3CN, followed by heating to 70°C for 12 hours, the mixture of diastereomers was transformed to cleanly generate a new set of signals attributed to $\mathbf{G1}\subset\boldsymbol{T_S}$-**1** (Figure 1c). The encapsulation of a single adamantane molecule was confirmed by integration of the upfield-shifted bound guest peaks in the ^{1}H NMR spectrum, and the observation of a 1/1 **1**·**G1** complex by high-resolution mass spectrometry (HRMS, Figure S106). The ^{1}H NMR spectrum of $\mathbf{G1}\subset\boldsymbol{T_S}$-**1** closely matches that of Et-containing $\boldsymbol{T_S}$-**2** (Figure 1c), in further support of this stereochemical assignment. Thus, a single equivalent of adamantane drives the transformation of **1** from a mixture of isomers featuring predominantly $\boldsymbol{T_L}$-**1**, into the otherwise minor $\boldsymbol{T_S}$-**1**. We attribute the strong binding ($K_a \approx 10^6$ M^{-1}, see Supporting Information, section 3) that underlies this transformation to extensive London dispersion forces between adamantane and the twelve endohedral methyl groups surrounding it.[38, 39]

Remarkably, when $\mathbf{G1}\subset\boldsymbol{T_S}$-**1** was treated with excess adamantane and the mixture was heated to 70°C, a second transformation occurred, yielding $\mathbf{G1}_4\subset\boldsymbol{T_L}$-**1**, where the configuration of **1** reverted to $\boldsymbol{T_L}$-**1**, capable of accommodating four adamantane molecules in its cavity. $\mathbf{G1}_4\subset\boldsymbol{T_L}$-**1** also formed spontaneously when excess adamantane was added to **1** at room temperature, along with residual low-symmetry diastereomers that equilibrated upon heating (Figure 1d). The slow-exchange encapsulation of four adamantane molecules in $\mathbf{G1}_4\subset\boldsymbol{T_L}$-**1** was confirmed by integration of the ^{1}H NMR spectrum and HRMS (Figures S11, S107). Treating **1** with smaller amounts of **G1** yielded mixtures of $\mathbf{G1}\subset\boldsymbol{T_S}$-**1** and $\mathbf{G1}_4\subset\boldsymbol{T_L}$-**1** (Figure S19). The ratio between integrals of peaks corresponding to bound **G1** and $\boldsymbol{T_L}$-**1** exceeds 3.5/1 even with a relatively small excess of added **G1** (≥3 equivalents), indicating positively cooperative binding (Figure S20).[40] Thus, the stereochemistry of **1** can be quantitatively toggled between $\boldsymbol{T_L}$ and $\boldsymbol{T_S}$ simply by varying the stoichiometry of added adamantane (Figure 1d). Although cages that encapsulate multiple guest molecules are well-known,[41-43] the efficient stoichiometry-dependent stereochemical switching displayed by host **1** is unprecedented.

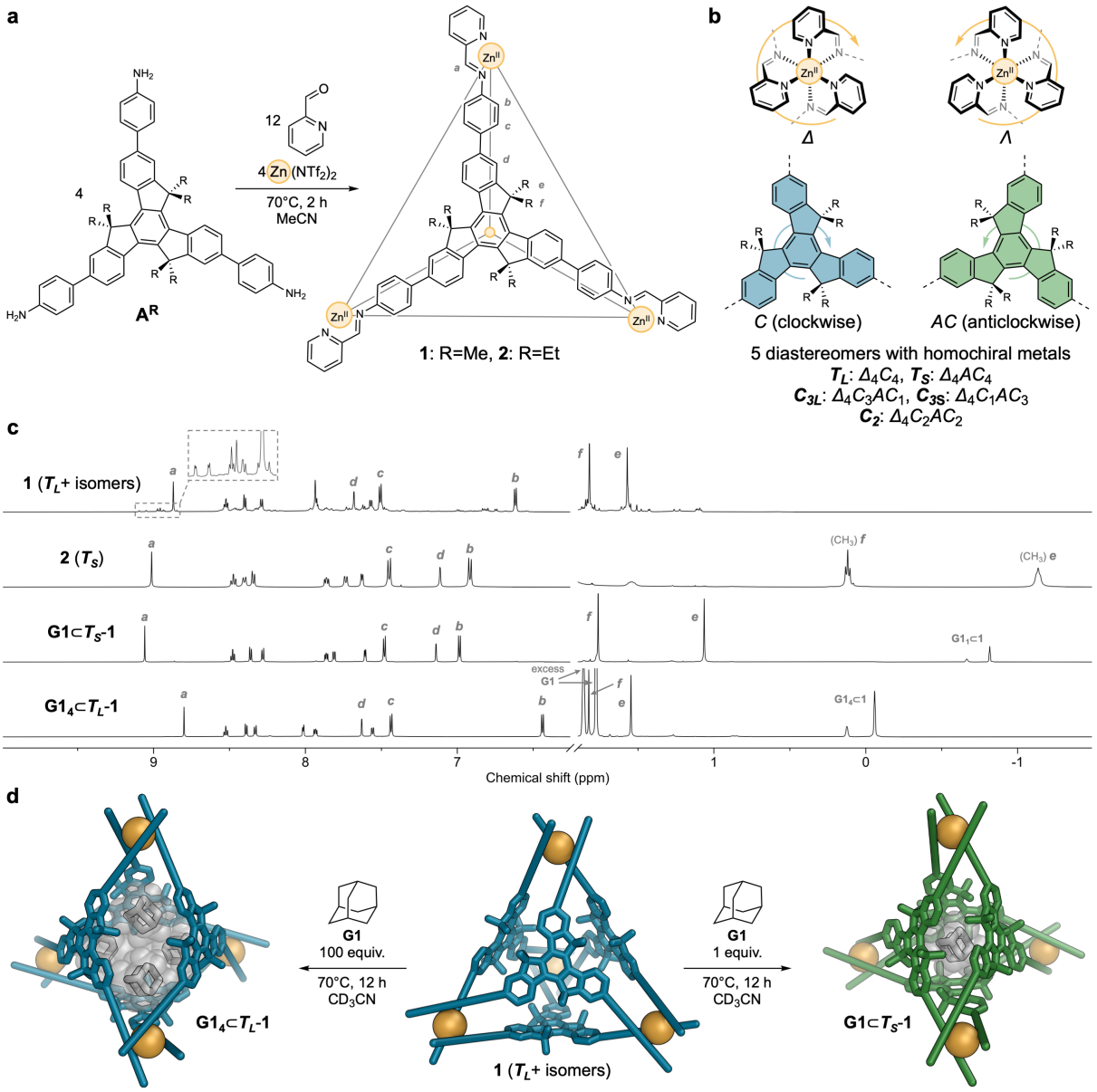

Figure 1. a. Subcomponent self-assembly of Zn_4L_4 cages **1** and **2**. **b.** Two types of stereogenic centers—the metals and faces of the cage—can give rise to 19 possible stereoisomers (Supporting Information, section 8). The five diastereomers featuring homochiral metals are listed. **c.** The distinct ^{1}H NMR spectra of cages **1** and **2** reflect their differing relative stereochemistry. Additionally, **1** exists as a mixture with several low-symmetry diastereomers. **d.** Different amounts of adamantane switch the stereochemistry of **1** to optimize binding.

A diverse range of guests were found to be encapsulated by **1** and influence its isomer distribution (Figure 2). Cyclohexane (**G2**) displayed similar behavior to adamantane, albeit with lower selectivity and binding affinity, where either **G2**$_5$⊂***T*$_L$-**1** or **G2**⊂***T*$_S$-**1** predominated in the presence of a large excess (500 equiv.) of **G2** or upon heating with a smaller excess (50 equiv.) of **G2**, respectively (Figures S74-S78). Cycloheptane (**G3**) and cyclooctane (**G4**) initially bound to ***T*$_L$-**1** but favored ***T*$_S$-**1** upon thermal equilibration (Figures S79-S80). Likewise, aliphatic guests of lower symmetry (**G5-G7**) templated the formation of ***T*$_S$-**1** (Figures S81-S83). Small aromatic guests such as fluorobenzene (**G8**), toluene (**G9**) and fluorene (**G10**) led to slight shifts of the ^{1}H NMR peaks corresponding to ***T*$_L$-**1**, indicating fast-exchange binding, but did not affect the isomer distribution (Figures S84-S89). Benzene (**G11**), in contrast, templated the formation of a C_3-symmetric isomer of **1** (Figures S57-S64), as did the larger triphenylmethane (**G12**, Figures S90-S91) and triphenylsilane (**G13**, Figures S48-S56). Guests containing multiple aromatic units, even the tetrahedral tetraphenylmethane (**G14**, Figures S92-S93),

favored the formation of a C_2-symmetric diastereomer of **1**. The pesticide mirex (**G17**), a bioaccumulative pollutant, bound to $\boldsymbol{T_L}$-**1** and a minor amount of $\boldsymbol{T_S}$-**1** (Figures S65-S73).

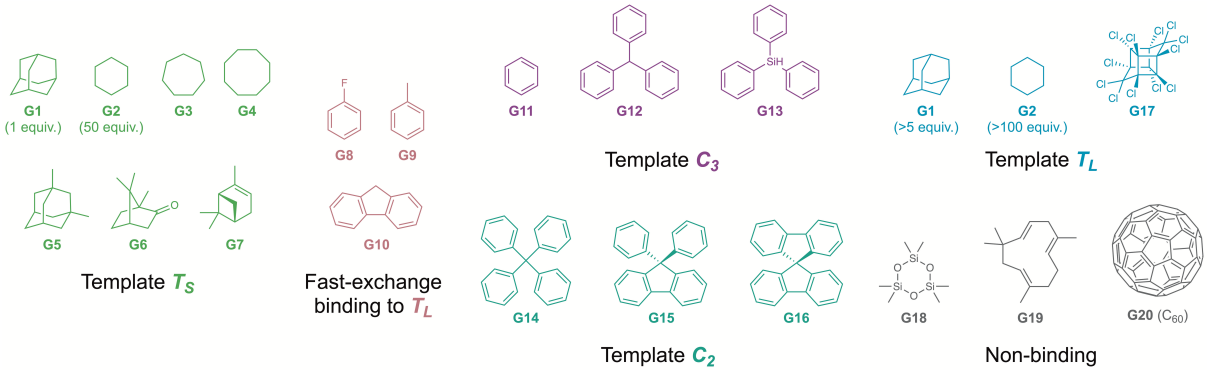

Figure 2. Summary of guests tested for binding within **1**, grouped by their stereochemical influence.

Partial ^{1}H NMR spectra of three selected low-symmetry host-guest complexes are shown in Figure 3a, with the imine and methyl regions highlighted. A large excess (600 equivalents) of benzene (**G11**) was found to drive the formation of a C_3-symmetric diastereomer, characterized by four imine signals and eight methyl peaks, which bound benzene with fast exchange. Triphenylsilane (**G13**) also templated the formation of a C_3-symmetric isomer, where peaks corresponding to a single encapsulated **G13** molecule were observed (Figures S48-S56). The relatively voluminous **G13** is best accommodated by the $\Delta_4C_3AC_1$ isomer, labelled $\boldsymbol{C_{3L}}$-**1**, the larger of the two possible C_3-symmetric isomers, rather than the smaller $\Delta_4C_1AC_3$ isomer, $\boldsymbol{C_{3S}}$-**1** (Table S2, Figure S118). We therefore assign the structure of the complex as **G13**$\subset\boldsymbol{C_{3L}}$-**1**. Since we could not observe bound-guest ^{1}H NMR peaks for benzene, nor detect its complexes with **1** by HRMS, we could not conclusively determine whether it templates $\boldsymbol{C_{3S}}$-**1** or $\boldsymbol{C_{3L}}$-**1**. Guest substitution experiments (Figures S100-S101), however, point to the latter possibility, with $\boldsymbol{C_{3L}}$-**1** likely accommodating multiple benzene molecules.

9,9-Spirobifluorene (**G16**) templated a C_2-symmetric diastereomer of **1** (Figures S30-S47), featuring six imine peaks and twelve well-resolved methyl peaks, ranging from 0.39 to 2.65 ppm in the ^{1}H NMR spectrum (Figure 3a, bottom). To the best of our knowledge, this is the first reported example of a C_2-symmetric diastereomer of a homoleptic tetrahedral cage. Whereas free **G16** (D_{2d} symmetry) displayed four ^{1}H NMR signals between 7.95 and 6.61 ppm, encapsulation in the cavity of $\boldsymbol{C_2}$-**1** led to its desymmetrization, resulting in eight broad signals (Figure 3b), shifted upfield by as much as 2.78 ppm relative to the free guest. These signals sharpened when the spectrum was acquired at –15°C, and partially coalesced at 70°C. In the C_2-symmetric cavity, the symmetry of **G16** decreases from D_{2d} to D_2, and the two otherwise homotopic benzene rings of each fluorene unit become diastereotopic, resulting in two distinct environments for each proton type (Figure 3c). A 180° rotation of the guest inside the cavity results in exchange between the two environments, giving rise the observed coalescence behavior. ROESY NMR experiments (Figures S38-S44) provided detailed information about the orientation of **G16** relative to the low-symmetry host and helped rule out a co-conformation where the principal C_2 axis of the guest (passing through both fluorene ring systems) is aligned with the C_2 axis of the cage framework.

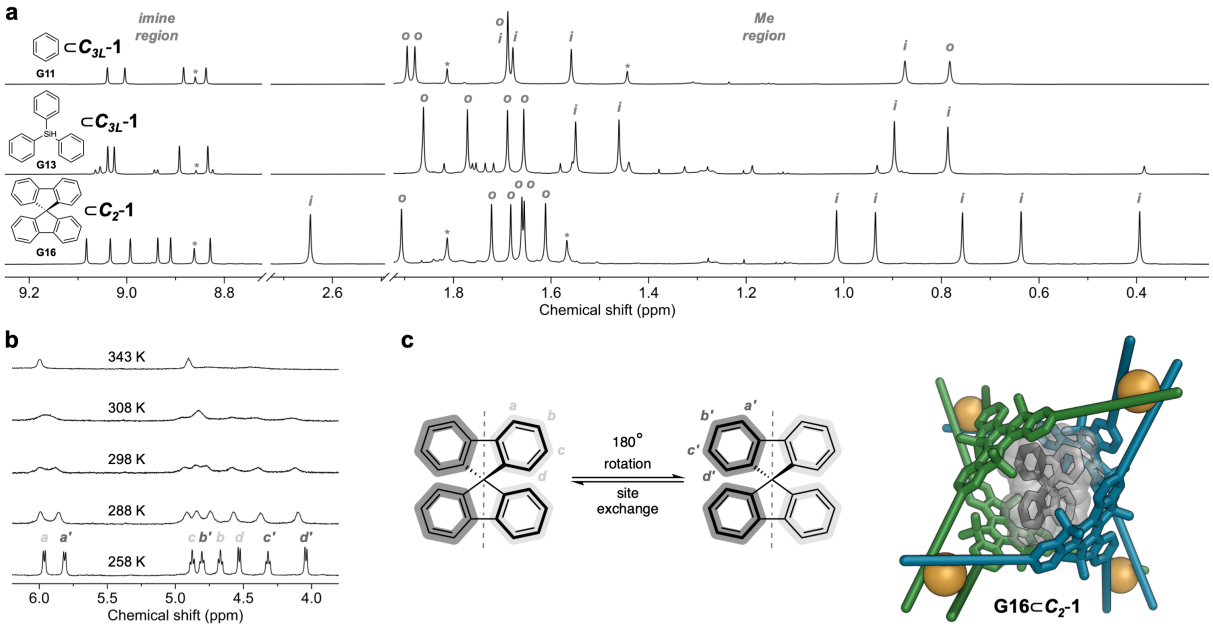

Figure 3. a. Highlights of the imine and methyl regions in ^{1}H NMR spectra of three selected low-symmetry host-guest complexes. Inward- and outward-pointing methyl groups are marked with ***i*** and ***o***, respectively. **b.** Bound-guest region of the ^{1}H NMR spectra of **G16**⊂***C*$_2$-**1** acquired at various temperatures. **c.** Illustration of the exchange between the two environments in bound **G16**, and a molecular model of **G16**⊂***C*$_2$-**1**.

Although we were unsuccessful in obtaining single crystals of low-symmetry host-guest complexes suitable for X-ray diffraction, several independent observations allowed us to establish the stereochemistry of the low-symmetry diastereomers described above. Firstly, along with a previously reported crystal structure corresponding to the predominant Δ_4C_4 (***T*$_L$**) configuration of **1** observed in solution,[37] we obtained a crystal grown under different conditions (Supporting Information, section 6), which contained a mixture of $\Delta_4C_3AC_1$ (***C*$_{3L}$-1**) and $\Delta_4C_2AC_2$ (***C*$_2$-1**) isomers. These structures demonstrate that the stereochemical flexibility of **1** stems from its ability to adopt heterochiral faces, rather than vertices. In addition, computational assessment (GFN2-xTB[44]) of the stability of low-symmetry isomers with heterochiral metals (e.g. $\Delta_3\Lambda_1C_4$, $\Delta_2\Lambda_2C_4$) versus heterochiral faces (e.g. $\Delta_4C_3AC_1$, $\Delta_4C_2AC_2$) showed that the latter are consistently lower in energy (Table S1), in line with the observed crystal structures.

Complementary insight into the structures of the diastereomers of **1** was provided by cyclic ion mobility-mass spectrometry (cIMS-MS, Supporting Information, section 7).[45] Ion mobility spectrometry can separate isomeric ions according to their shape and size (as reflected in collisional cross-section values).[46-48] Compared to more common ion mobility techniques, cyclic ion-mobility (cIMS) achieves uniquely high resolution by repeatedly passing the analyte ions through a cyclic racetrack, thus significantly increasing their pathlength. From a sample of guest-free **1**, the [**1**]$^{8+}$ ion was mass-selected and analyzed by cIMS. Figure 4a shows three mobilograms of [**1**]$^{8+}$ with different numbers of passes through the cIMS racetrack. The mobilogram obtained with 10 passes clearly shows the presence of five isomers, in agreement with the ^{1}H NMR data. Moreover, the arrival times and relative intensities of the signals indicate the relative population of the diastereomers: the peak with the longest arrival time corresponds to the largest isomer, ***T*$_L$**, and possesses the largest intensity, in agreement with the ^{1}H NMR spectrum of **1**. The major ***T*$_L$** is followed in intensity by ***C*$_{3L}$**, ***C*$_2$**, ***C*$_{3S}$**, and ***T*$_S$**, which have progressively smaller molecular volumes (Table S2). A 9.9/5.2/2.6/1.8/1 ***T*$_L$**/***C*$_{3L}$**/***C*$_2$**/***C*$_{3S}$**/***T*$_S$** ratio is extracted by integrating the peaks in the mobilogram (neglecting differences in relative response factors between the isomers).

Next, the host-guest complexes of **1** were analyzed by cIMS, as mass-selected [**G**⊂**1**]$^{8+}$ ions (Figure 4b, left). The resulting mobilograms corroborate the assignments from ^{1}H NMR: adamantane (**G1**, 1 equiv.) and cyclooctane (**G4**) template the formation of the smallest diastereomer—***T*$_S$-1**, whereas an excess of adamantane templates the formation of **G1**$_4$⊂***T*$_L$-1**, which can be inferred to expand upon

encapsulation of four **G1** molecules, as indicated by the longer arrival time compared to free [$\boldsymbol{T_L}$-**1**]$^{8+}$. Mirex (**G17**) also templates $\boldsymbol{T_L}$-**1**, along with a minor amount of an additional isomer, identified as $\boldsymbol{T_S}$-**1** by ^{1}H NMR (which indicated the formation of two *T*-symmetric complexes, Figure S66). The cavity of $\boldsymbol{T_S}$-**1** must expand significantly to accommodate the relatively large **G17**, in line with the longer arrival time for **G17**⊂$\boldsymbol{T_S}$-**1** compared to complexes of smaller guests, such as **G1**⊂$\boldsymbol{T_S}$-**1** and **G4**⊂$\boldsymbol{T_S}$-**1**. Complexes of $\boldsymbol{C_{3L}}$-**1** and $\boldsymbol{C_2}$-**1**, favored by **G12**/**G13** and **G16**, respectively, were clearly resolved, though only differing by the *C*/*AC* configuration of a single truxene face, highlighting the potential of cIMS in analyzing mixtures of subtly different isomers.

cIMS-MS also provided a unique method to study the dynamics of the host-guest complexes upon release of the guest, namely through the fragmentation of the [**G**⊂**1**]$^{8+}$ ions. Following mass-selection of [**G**⊂**1**]$^{8+}$, collision-induced dissociation (CID) prior to cIMS separation results in guest release, generating [**1**]$^{8+}$ ions that can be analyzed by cIMS. If guest release would induce complete scrambling of the stereochemical information of the host, the mobilograms of [**1**]$^{8+}$ generated by guest release would be expected to be identical to that derived from a sample of guest-free **1**. In contrast, deviation from the isomer distribution of guest-free **1** would indicate that the stereochemical information templated by the guest is retained upon its release. The mobilograms in Figure 4b (right) overwhelmingly point to the latter scenario—**1** retains its stereochemistry following guest release. For example, comparing the mobilograms resulting from loss of **G1** and **G4** from $\boldsymbol{T_S}$-**1**, it can be inferred that **G4** is released through a mechanism which does not require significant reorganization of the host, as the mobilogram still shows mostly $\boldsymbol{T_S}$-**1**. In contrast, release of the more spherical and strongly binding **G1** leads to almost complete equilibration of **1** back to the original isomer distribution, indicating a release mechanism proceeding with a larger extent of host dissociation. Apart from **G1**, however, all other guests were found to be released while **1** retained an isomer distribution remarkably close to that of the parent host-guest complexes, even though all guests apart from **G4** are much larger than the portals at the cage edges, hence requiring substantial reorganization of the host to exit the cavity. These results thus indicate a "shape-memory" phenomenon, where the cage retains an out-of-equilibrium isomer distribution following the release of template guests.[49-52]

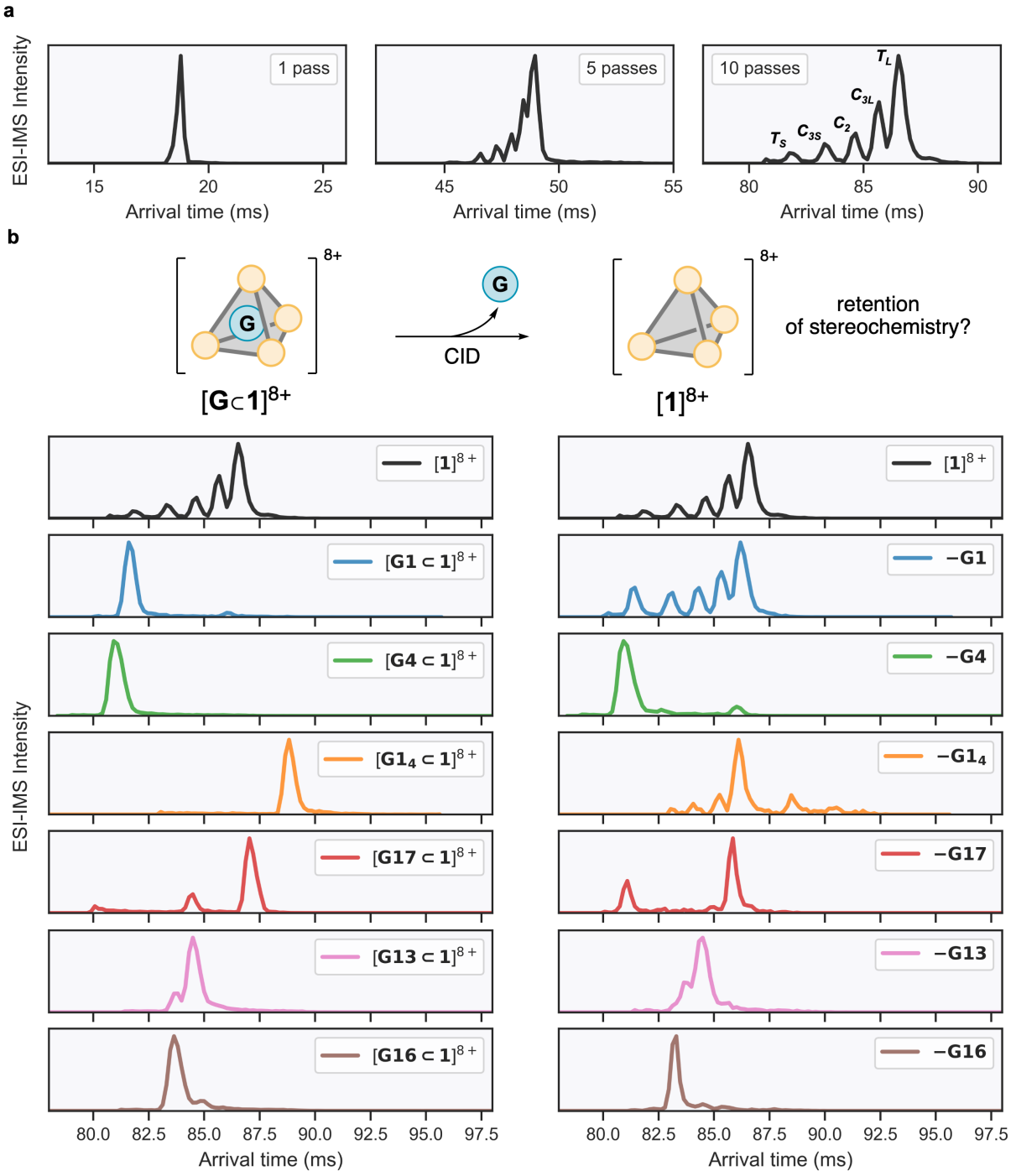

Figure 4. cIM-MS studies of **1** and its host-guest complexes. **a.** The five diastereomers of **1** can be resolved by cIMS. **b.** Mobilograms of host-guest complexes (left) corroborate the stereochemical preference inferred by ^{1}H NMR. MS-MS fragmentation of the $[\mathbf{G}\subset\mathbf{1}]^{8+}$ ions to release bound guest, followed by cIMS analysis of the nascent $[\mathbf{1}]^{8+}$ ions, show that the guest-templated stereochemistry is retained following guest release.

Figure 5 depicts two manifestations of this feature in solution. Competitive binding experiments between cyclohexane (**G2**) and adamantane (**G1**) (Figures S96-S97) yielded $\mathbf{G1}_4\subset\boldsymbol{T_L}$-**1** as the thermodynamic product (Figure 5a). However, if the weaker-binding cyclohexane was added first, to form $\mathbf{G2}_5\subset\boldsymbol{T_L}$-**1**, and excess adamantane was added subsequently, $\mathbf{G1}_4\subset\boldsymbol{T_L}$-**1** was not generated immediately, as would be expected if guest exchange proceeded with a substantial degree of host dissociation. Instead, over the course of weeks at room temperature, mixed cyclohexane/adamantane complexes could be observed by ^{1}H-NMR (Figures S98-S99), which slowly converted to the thermodynamic $\mathbf{G1}_4\subset\boldsymbol{T_L}$-**1**. The ability to generate such metastable mixed-guest

complexes might find use in promoting intermolecular reactions within the cavity of **1** and controlling their selectivity.[53-55]

In a second competitive binding experiment, an equimolar mixture of mirex (**G17**) and cyclooctane (**G4**) was added to empty **1** (Figures S102-S103). The larger mirex was selectively bound by the major T_L-**1**, leaving the smaller cyclooctane in solution. Alternatively, if empty **1** was first treated with cyclohexane and heated to 70°C for 12 hours, the stereochemistry of **1** was "molded" to T_S. Upon addition of the same **G4**/**G17** mixture, the smaller **G4** was bound selectively (displacing **G2**), leaving **G17** in bulk solution. Thus, **1** can be programmed to extract either guest from the mixture, by templating its stereochemistry with a displaceable guest. This preliminary experiment demonstrates that hosts with programmable stereochemistry can be employed to extract different guests from a mixture at will, instead of employing multiple different hosts specifically designed for each guest.

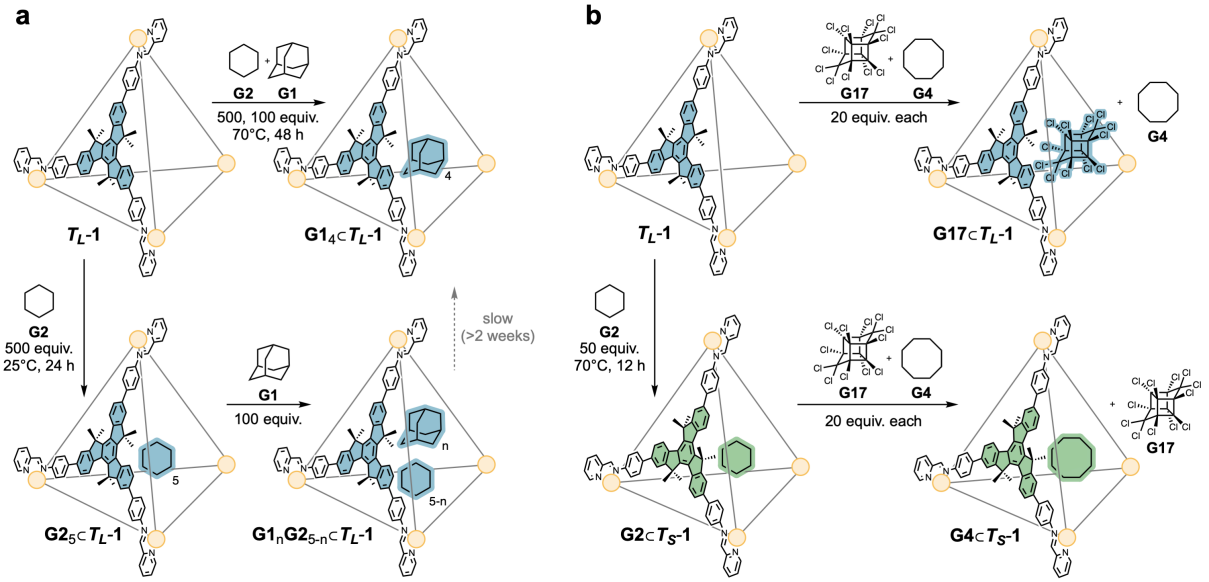

Figure 5. a. 1 binds adamantane (**G1**) more strongly than cyclohexane (**G2**), but the displacement of **G2** by **G1** proceeds slowly, through far-from-equilibrium mixed-guest complexes. **b.** Adding a mixture of a large guest (mirex, **G17**) and a small guest (cyclooctane, **G4**) to empty **1** (predominantly T_L) results in selective encapsulation of **G17**. In contrast, if **G2** is first used to template the transformation of **1** to T_S stereochemistry, addition of the same mixture of guests results in the selective encapsulation of **G4**.

Conclusion

Host **1** displays remarkable stereochemical flexibility, both in terms of the number of accessible isomers and the selectivity with which each isomer can be favored. We show that this flexibility stems from the ability of the cage framework to feature mixed *clockwise* and *anticlockwise* truxene faces, as supported by crystallography and computational studies. Cyclic ion mobility-mass spectrometry reinforced the stereochemical analysis of host-guest complexes and was uniquely effective in probing the mechanism of guest release, indicating that the stereochemical information templated by a guest can be retained upon its release. This property of host **1** enabled the preparation of far-from-equilibrium mixed-guest complexes, and the programable binding of guests from a mixture.

Further refinement of the design principles that give rise to stereochemically plastic cages, along with methods to study their dynamics, could lead to programmable supramolecular hosts of utility in advanced purification and catalysis applications.

Acknowledgments

I.M. gratefully acknowledges a Herchel Smith Postdoctoral Fellowship. P.C.P.T. acknowledges the Engineering and Physical Sciences Research Council via project EP/S024220/1 EPSRC Center for Doctoral Training in Automated Chemical Synthesis Enabled by Digital Molecular Technologies. The UMONS MS laboratory acknowledges FRS-FNRS for the financial support for the acquisition of the cIMS mass spectrometer (INFRA-GEQ U.GOO2.25). Q.D. is an FNRS postdoctoral fellow and C.L. is an FNRS doctoral fellow.

References

(1) Constable, E. C. Stereogenic metal centres–from Werner to supramolecular chemistry. *Chem. Soc. Rev.* **2013**, *42*, 1637-1651.
(2) Zhu, H.; Speakman, N. M.; Ronson, T. K.; Nitschke, J. R. Higher-order Cu^{I}-Based cages via subcomponent self-assembly. *Acc. Chem. Res.* **2025**, *58*, 1296-1307.
(3) Liu, T.; Liu, Y.; Xuan, W.; Cui, Y. Chiral nanoscale metal–organic tetrahedral cages: Diastereoselective self-assembly and enantioselective separation. *Angew. Chem. Int. Ed.* **2010**, *49*, 4121-4124.
(4) Bolliger, J. L.; Belenguer, A. M.; Nitschke, J. R. Enantiopure water-soluble $[Fe_4L_6]$ cages: host–guest chemistry and catalytic activity. *Angew. Chem. Int. Ed.* **2013**, *52*, 7958-7962.
(5) Chen, L.-J.; Yang, H.-B.; Shionoya, M. Chiral metallosupramolecular architectures. *Chem. Soc. Rev.* **2017**, *46*, 2555-2576.
(6) Dong, J.; Liu, Y.; Cui, Y. Supramolecular chirality in metal–organic complexes. *Acc. Chem. Res.* **2020**, *54*, 194-206.
(7) Zou, Y.-Q.; Zhang, D.; Ronson, T. K.; Tarzia, A.; Lu, Z.; Jelfs, K. E.; Nitschke, J. R. Sterics and hydrogen bonding control stereochemistry and self-sorting in BINOL-based assemblies. *J. Am. Chem. Soc.* **2021**, *143*, 9009-9015.
(8) Yang, Y.; Ronson, T. K.; Lu, Z.; Zheng, J.; Vanthuyne, N.; Martinez, A.; Nitschke, J. R. A curved host and second guest cooperatively inhibit the dynamic motion of corannulene. *Nat. Commun.* **2021**, *12*, 4079.
(9) Séjourné, S.; Labrunie, A.; Dalinot, C.; Canevet, D.; Guechaichia, R.; Bou Zeid, J.; Benchohra, A.; Cauchy, T.; Brosseau, A.; Allain, M.; et al. Chiral Truxene-Based Self-Assembled Cages: Triple Interlocking and Supramolecular Chirogenesis. *Angew. Chem. Int. Ed.* **2024**, *63*, e202400961.
(10) Young, M. C.; Holloway, L. R.; Johnson, A. M.; Hooley, R. J. A Supramolecular Sorting Hat: Stereocontrol in Metal–Ligand Self-Assembly by Complementary Hydrogen Bonding. *Angew. Chem. Int. Ed.* **2014**, *53*, 9832-9836.
(11) Mosquera, J.; Ronson, T. K.; Nitschke, J. R. Subcomponent Flexibility Enables Conversion between D4-Symmetric $Cd^{II}_8L_8$ and T-Symmetric $Cd^{II}_4L_4$ Assemblies. *J. Am. Chem. Soc.* **2016**, *138*, 1812-1815.
(12) Lewis, J. E.; Crowley, J. D. Metallo-Supramolecular Self-Assembly with Reduced-Symmetry Ligands. *ChemPlusChem* **2020**, *85*, 815-827.
(13) Zhang, D.; Ronson, T. K.; Güryel, S. l.; Thoburn, J. D.; Wales, D. J.; Nitschke, J. R. Temperature controls guest uptake and release from Zn_4L_4 tetrahedra. *J. Am. Chem. Soc.* **2019**, *141*, 14534-14538.
(14) Ronson, T. K.; Carpenter, J. P.; Nitschke, J. R. Dynamic optimization of guest binding in a library of diastereomeric heteroleptic coordination cages. *Chem* **2022**, *8*, 557-568.
(15) Tripathy, D.; Debata, N. B.; Naik, K. C.; Sahoo, H. S. Coordination driven discrete metallopolygons and cages from unsymmetric bidentate ligands. *Coord. Chem. Rev.* **2022**, *456*, 214396.
(16) Xu, C.; Lin, Q.; Shan, C.; Han, X.; Wang, H.; Wang, H.; Zhang, W.; Chen, Z.; Guo, C.; Xie, Y.; et al. Metallo-Supramolecular Octahedral Cages with Three Types of Chirality towards Spontaneous Resolution. *Angew. Chem. Int. Ed.* **2022**, *61*, e202203099.
(17) Davies, J. A.; Tarzia, A.; Ronson, T. K.; Auras, F.; Jelfs, K. E.; Nitschke, J. R. Tetramine Aspect Ratio and Flexibility Determine Framework Symmetry for Zn_8L_6 Self-Assembled Structures. *Angew. Chem. Int. Ed.* **2023**, *62*, e202217987.
(18) Molinska, P.; Tarzia, A.; Male, L.; Jelfs, K. E.; Lewis, J. E. M. Diastereoselective Self-Assembly of Low-Symmetry Pd_nL_{2n} Nanocages through Coordination-Sphere Engineering. *Angew. Chem. Int. Ed.* **2023**, *62*, e202315451.
(19) Neukirch, L.; Clever, G. H. Topological variety and self-sorting in homo- and heteroleptic Pd_nL_{2n} metallo-supramolecular assemblies. *Chem. Sci.* **2025**, *16*, 12242-12276.

(20) Gome, J. A.; Avery, Z. T.; Lawson, N. R.; Stansfield, O. G.; Evans, J. D.; Gardiner, M. G.; Connell, T. U.; Preston, D. Low-Symmetry Face-Capped Fe(II) Tetrahedra Through Anisotropic Ligand Extension. *Angew. Chem. Int. Ed.* **2025**, *64*, e202503473.
(21) Chakrabarty, R.; Mukherjee, P. S.; Stang, P. J. Supramolecular coordination: self-assembly of finite two- and three-dimensional ensembles. *Chem. Rev.* **2011**, *111*, 6810-6918.
(22) Castilla, A. M.; Ramsay, W. J.; Nitschke, J. R. Stereochemistry in subcomponent self-assembly. *Acc. Chem. Res.* **2014**, *47*, 2063-2073.
(23) McConnell, A. J. Metallosupramolecular cages: from design principles and characterisation techniques to applications. *Chem. Soc. Rev.* **2022**, *51*, 2957-2971.
(24) Martín Díaz, A. E.; Lewis, J. E. M. Structural Flexibility in Metal-Organic Cages. *Front. Chem.* **2021**, *9*, 706462.
(25) Hema, K.; Grommet, A. B.; Białek, M. J.; Wang, J.; Schneider, L.; Drechsler, C.; Yanshyna, O.; Diskin-Posner, Y.; Clever, G. H.; Klajn, R. Guest encapsulation alters the thermodynamic landscape of a coordination host. *J. Am. Chem. Soc.* **2023**, *145*, 24755-24764.
(26) Banerjee, R.; Bhandari, P.; Hickey, N.; Mukherjee, P. S. Guest-Shape-Directed Structural Switching between Two Isomers of a Pd_6 Host and Its Structural Adaptability for Selective Photodimerization. *J. Am. Chem. Soc.* **2025**, *147*, 23049-23059.
(27) Chen, H.; Abe, T.; Chai, R.; Hiraoka, S. Selection of self-assembled configurational isomers from a dynamic library via a multivariant optimization process. *Nat. Commun.* **2025**, *16*, 4387.
(28) Xu, H.; Ronson, T. K.; Heard, A. W.; Teeuwen, P. C.; Schneider, L.; Pracht, P.; Thoburn, J. D.; Wales, D. J.; Nitschke, J. R. A pseudo-cubic metal–organic cage with conformationally switchable faces for dynamically adaptive guest encapsulation. *Nat. Chem.* **2025**, *17*, 289-296.
(29) Rizzuto, F. J.; Nitschke, J. R. Stereochemical plasticity modulates cooperative binding in a $Co^{II}_{12}L_6$ cuboctahedron. *Nat. Chem.* **2017**, *9*, 903-908.
(30) Hong, C. M.; Kaphan, D. M.; Bergman, R. G.; Raymond, K. N.; Toste, F. D. Conformational selection as the mechanism of guest binding in a flexible supramolecular host. *J. Am. Chem. Soc.* **2017**, *139*, 8013-8021.
(31) Xue, W.; Wu, K.; Ouyang, N.; Brotin, T.; Nitschke, J. R. Allosterically regulated guest binding determines framework symmetry for an $Fe^{II}_4L_4$ cage. *Angew. Chem. Int. Ed.* **2023**, *62*, e202301319.
(32) Speakman, N. M.; Heard, A. W.; Nitschke, J. R. A $Cu^{I}_6L_4$ cage dynamically reconfigures to form suit[4]anes and selectively bind fluorinated steroids. *J. Am. Chem. Soc.* **2024**, *146*, 10234-10239.
(33) Zhang, D.; Ronson, T. K.; Zou, Y.-Q.; Nitschke, J. R. Metal–organic cages for molecular separations. *Nat. Rev. Chem.* **2021**, *5*, 168-182.
(34) Bogie, P. M.; Miller, T. F.; Hooley, R. J. Synthesis and Applications of Endohedrally Functionalized Metal-Ligand Cage Complexes. *Isr. J. Chem.* **2019**, *59*, 130-139.
(35) Platzek, A.; Juber, S.; Yurtseven, C.; Hasegawa, S.; Schneider, L.; Drechsler, C.; Ebbert, K. E.; Rudolf, R.; Yan, Q.-Q.; Holstein, J. J.; et al. Endohedrally Functionalized Heteroleptic Coordination Cages for Phosphate Ester Binding. *Angew. Chem. Int. Ed.* **2022**, *61*, e202209305.
(36) Zhu, J.-L.; Zhang, D.; Ronson, T. K.; Wang, W.; Xu, L.; Yang, H.-B.; Nitschke, J. R. A Cavity-Tailored Metal-Organic Cage Entraps Gases Selectively in Solution and the Amorphous Solid State. *Angew. Chem. Int. Ed.* **2021**, *60*, 11789-11792.
(37) Massad, I.; Dobson, J.; Teeuwen, P.; Ronson, T.; Nitschke, J. London dispersion governs stereochemistry, stability, and self-sorting in a system of M_4L_4 cages. *ChemRxiv* **2026**, doi: 10.26434/chemrxiv-22026-klf26450.
(38) Schneider, H.-J. Binding Mechanisms in Supramolecular Complexes. *Angew. Chem. Int. Ed.* **2009**, *48*, 3924-3977.
(39) Echeverría, J.; Aullón, G.; Danovich, D.; Shaik, S.; Alvarez, S. Dihydrogen contacts in alkanes are subtle but not faint. *Nat. Chem.* **2011**, *3*, 323-330.
(40) Hunter, C. A.; Anderson, H. L. What is Cooperativity? *Angew. Chem. Int. Ed.* **2009**, *48*, 7488-7499.
(41) Fujita, M.; Oguro, D.; Miyazawa, M.; Oka, H.; Yamaguchi, K.; Ogura, K. Self-assembly of ten molecules into nanometre-sized organic host frameworks. *Nature* **1995**, *378*, 469-471.
(42) Rebek Jr., J. Simultaneous Encapsulation: Molecules Held at Close Range. *Angew. Chem. Int. Ed.* **2005**, *44*, 2068-2078.
(43) Rizzuto, F. J.; von Krbek, L. K.; Nitschke, J. R. Strategies for binding multiple guests in metal–organic cages. *Nat. Rev. Chem.* **2019**, *3*, 204-222.

(44) Bannwarth, C.; Ehlert, S.; Grimme, S. GFN2-xTB—An accurate and broadly parametrized self-consistent tight-binding quantum chemical method with multipole electrostatics and density-dependent dispersion contributions. *J. Chem. Theory. Comput.* **2019**, *15*, 1652-1671.
(45) Giles, K.; Ujma, J.; Wildgoose, J.; Pringle, S.; Richardson, K.; Langridge, D.; Green, M. A cyclic ion mobility-mass spectrometry system. *Anal. Chem.* **2019**, *91*, 8564-8573.
(46) Kalenius, E.; Groessl, M.; Rissanen, K. Ion mobility–mass spectrometry of supramolecular complexes and assemblies. *Nat. Rev. Chem.* **2019**, *3*, 4-14.
(47) Geue, N. Modern Electrospray Ionization Mass Spectrometry Techniques for the Characterization of Supramolecules and Coordination Compounds. *Anal. Chem.* **2024**, *96*, 7332-7341.
(48) Geue, N.; Winpenny, R. E. P.; Barran, P. E. Ion Mobility Mass Spectrometry for Large Synthetic Molecules: Expanding the Analytical Toolbox. *J. Am. Chem. Soc.* **2024**, *146*, 8800-8819.
(49) Choi, D.-S.; Chong, Y. S.; Whitehead, D.; Shimizu, K. D. Molecules with Shape Memory Based on Restricted Rotation. *Org. Lett.* **2001**, *3*, 3757-3760.
(50) Chong, Y. S.; Smith, M. D.; Shimizu, K. D. A Conformationally Programmable Ligand. *J. Am. Chem. Soc.* **2001**, *123*, 7463-7464.
(51) Rasberry, R. D.; Shimizu, K. D. Molecular playdough: conformationally programmable molecular receptors based on restricted rotation. *Org. Biomol. Chem.* **2009**, *7*, 3899-3905.
(52) Zhang, D.; Ronson, T. K.; Greenfield, J. L.; Brotin, T.; Berthault, P.; Léonce, E.; Zhu, J.-L.; Xu, L.; Nitschke, J. R. Enantiopure [Cs^+/Xe⊂ Cryptophane]⊂ $Fe^{II}_4L_4$ Hierarchical Superstructures. *J. Am. Chem. Soc.* **2019**, *141*, 8339-8345.
(53) Brown, C. J.; Toste, F. D.; Bergman, R. G.; Raymond, K. N. Supramolecular Catalysis in Metal–Ligand Cluster Hosts. *Chem. Rev.* **2015**, *115*, 3012-3035.
(54) Morimoto, M.; Bierschenk, S. M.; Xia, K. T.; Bergman, R. G.; Raymond, K. N.; Toste, F. D. Advances in supramolecular host-mediated reactivity. *Nat. Catal.* **2020**, *3*, 969-984.
(55) Syntrivanis, L.-D.; Tiefenbacher, K. Reactivity Inside Molecular Flasks: Acceleration Modes and Types of Selectivity Obtainable. *Angew. Chem. Int. Ed.* **2024**, *63*, e202412622.